

METAL HYDRIDES : ACTIVATION PROCEDURES, THERMODYNAMICS AND KINETIC ANALYSIS

Pierre Millet, Michel Guymont

*Institut de Chimie Moléculaire et des Matériaux, UMR CNRS n° 8182, Université Paris sud 11,
15 rue Georges Clémenceau, 91405 Orsay cedex France*

ABSTRACT:

When put into contact with gaseous hydrogen, many elemental metals, alloys and intermetallic compounds (IMC) form metal hydrides at low or moderate pressure. This interesting property offers the possibility of reversibly storing large amounts of hydrogen, and storage reservoirs can be designed for miscellaneous applications. Although these solid-gas systems suffer from an unfavourable H-to-M weight ratio which still postpones the development of hydride-based hydrogen tanks for automotive applications, metal-hydride forming systems remain interesting for stationary applications. However, the thermodynamic and kinetic properties of most of these systems are complicated by hysteresis and for practical applications, it is necessary to develop activation procedures in order to optimize sorption capacities and kinetics. In this communication, the $\text{LaNi}_5\text{-H}_2(\text{g})$ system is more specifically considered. Thermodynamic states and sorption kinetics are analyzed during the activation process, in relation with particles size (decrepitation). It is shown how kinetic data can be collected using simple Sievert's-type gas distribution apparatus and how they can be analyzed in the frequency domain using pneumato-chemical impedance spectroscopy (PIS). Gas-phase impedance diagrams are measured as a function of the number of hydriding cycles and analyzed using a sorption mechanism in which two-steps, a surface chemisorption step and a bulk diffusion-controlled mass transport step, are considered.

KEYWORDS: *metal-hydrogen system; intermetallic compounds; frequency domain analysis; Fourier analysis.*

1. Introduction

Hydride forming metals, alloys or intermetallic compounds (IMC) can be used to reversibly store large amounts of hydrogen. Following the discovery of the hydrogen absorption properties of ZrNi [1] and LaNi_5 [2], a large number of compounds and alloys have been identified and characterized [3] and a large variety of processes based on hydride systems have been reported in the literature, for the development of hydrogen storage reactors but also for other applications such as heat pumps, refrigerators and hydride batteries. At the present time, hydride reservoirs of various shape (mostly bottles), operating over large domains of pressure (from a few mbar up to 20 bars at room temperature) and temperature (-20°C up to several hundred Celsius), having various capacities (from a few Nliters up to several Nm^3) are commercially available. Although hydride tanks suffer from an excessive weight for automotive applications (a few wt.% hydrogen can be reversibly stored whereas at least 6 wt.% is required), many of these systems are still interesting for stationary applications. In particular, they can be used in auxiliary power units to store hydrogen produced from renewable energy sources using a PEM water electrolyzer, as discussed in the proceedings of this Conference [4].

The thermodynamic and kinetic characterization of $\text{IMC-H}_2(\text{g})$ systems is complicated by the presence of an important hysteresis : the plateau pressure during absorption is significantly higher than the plateau pressure during desorption, indicating than non-reversible transformations are taking place. For an unactivated LaNi_5 powder sample, the difference between the two plateau pressures is significantly large (ca. 1400 mbar at 298 K). During the first hydriding cycles, the absorption plateau pressure decreases and the difference can be reduced down to ca. 400 mbar within 10 cycles. This process is known as decrepitation : the precipitation of the hydride phase produce significantly large internal strain and stresses which in turn pulverize the metallic samples. Average particle diameters of a few microns have been reported in the literature for activated samples. The purpose of this communication is to use pneumato-chemical impedance spectroscopy (PIS) [5,6] to analyze the kinetics of hydrogen sorption during the activation of the $\text{LaNi}_5\text{-H}_2(\text{g})$ system.

2. PIS analysis of sorption kinetics

2.1. Principles

Pneumato-chemical Impedance Spectroscopy (PIS) is a tool which can be used to analyze the kinetics of solid-gas reactions in the frequency (Fourier) domain [5]. This technique is an adaptation of the more popular Electrochemical Impedance Spectroscopy (EIS) which is used to determine the different steps involved in multi-step electrochemical transformations. Whereas most EIS experimental impedance spectra are obtained using harmonic potential perturbations (the system impedance is measured over a large frequency domain, frequency after frequency), experimental PIS spectra are obtained using appropriate non-harmonic pressure perturbations. The dynamics of the system (the H₂(g) absorbing material) is analyzed using the theory of systems. For a solid-gas reaction, the pneumato-chemical system (the term “pneumato” refers to gaseous hydrogen and the term “chemical” refers to the solid-state reaction between H₂(g) and the solid which leads to the formation of hydrogen solid solutions and hydrides) is linear and time invariant, and the relationships between time-dependent pressure (the input excitation $i(t)$) and H₂ mass flow (the output response $o(t)$) is a convolution [5]:

$$o(t) = \int_{-\infty}^{+\infty} i(\tau) h(t - \tau) d\tau = i(t) * h(t) \quad (1)$$

where $h(t)$ is the impulse response of the system when the unit impulse (Dirac) function $\delta(t)$ is applied as input :

$$\delta(t) \rightarrow h(t) \quad (2)$$

The interest of equation (1) is that $h(t)$ appears as a characteristic of the system under consideration, whatever the pairs $\{i(t); o(t)\}$ are. The determination of $h(t)$ is therefore very useful since, when it is known, (i) the response $o(t)$ to any given excitation $i(t)$ and (ii) the excitation $i(t)$ to any given response $o(t)$ can both be calculated. However, direct use of Eq. (1) is seldom found in the literature. Although Eq. (1) could be solved numerically, it is not easy from an experimental viewpoint to directly obtain $h(t)$ from Eq. (2) : this is because it is not simple (if possible) to generate a true Dirac excitation $\delta(t)$. This may be possible to a certain extent when $i(t)$ is an electric voltage, but not when $i(t)$ is a pressure, as discussed here : non-isothermal effects and time-lags due to gas compression produce more or less distorted pressure pulses. It is therefore much more convenient to analyze data in the Fourier domain where the convolution (1) becomes a simple algebraic product :

$$FT[i(t) * h(t)] = FT[i(t)] \cdot FT[h(t)] = FT[o(t)] \quad (3)$$

where $FT[i(t)]$ denotes the Fourier transform of $i(t)$.

It should be noted that the FT of the impulse response $h(t)$ is called the transfer function $H(f)$ of the system :

$$FT[h(t)] = H(f) = \int_{-\infty}^{+\infty} h(t) e^{-j\omega t} dt \quad (4)$$

where f is the frequency in Hz, $\omega = 2\pi f$ is the angular frequency in rad.s⁻¹.

More conveniently, Eq. (3) can be written in the form :

$$H(f) = \frac{FT[o(t)]}{FT[i(t)]} \quad (5)$$

From a dynamic viewpoint, the transfer function $H(f)$ of a system is like a fingerprint, in the sense that it is very characteristic of this system. $H(f)$ can be obtained in principle from Eq. (5) by taking the ratio of the FTs of any pair $\{i(t); o(t)\}$. $H(f)$ is defined over a frequency domain ranging from $f = 0$ HZ up to higher values, as long as the denominator is non-zero. In EIS, two different transfer functions are commonly used : the admittance $Y(\omega)$ which is defined as the (complex) ratio of the current to the voltage, and the reciprocal, the impedance $Z(\omega)$ which, according to Ohm's law, is defined as the (complex) ratio of the voltage to the resulting current. In PIS, pneumato-chemical impedances are measured from $\{i(t); o(t)\}$ pairs such as {pressure(t); mass flow(t)} signals, as described in the next sections.

2.2. Experimental setup

Gas transfer experiments were performed using the Sievert gas distribution apparatus (SGDA) pictured in figure 1. A detailed description of this setup can be found in Ref. [5]. Briefly, in a typical experiment, hydrogen amounts are transferred from the reference volume chamber Ch_1 to the reaction chamber Ch_2 (immersed in a thermostated bath) using different manual valves (MVs).

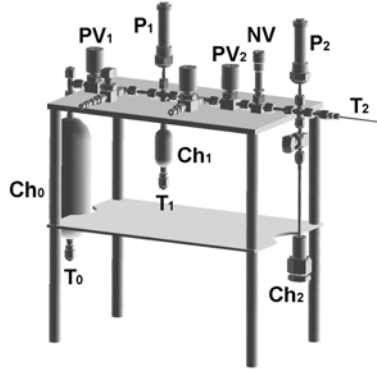


Figure 1 : schematic diagram of the experimental setup.



Figure 2 : photograph of the experimental setup used to measure PIS impedances.

The driving force to gas transfers is the initial pressure difference $\Delta P^0 = P_1^0 - P_2^0$. A needle valve (NV) with a metering tip is used to slow down the process in order to maintain isothermal conditions and avoid gas convection. Transient pressures $P_1(t)$ and $P_2(t)$ measured in both chambers are synchronously sampled until equilibrium is reached in the two chambers : they provide raw data for kinetic analysis.

2.3. Transfer functions of special interest on a SGDA

Different transfer functions can be obtained from time-domain experiments using a SGDA. In particular, the pneumato-chemical impedances relating pressure perturbations to gas flow responses (flow/force relationships) are interesting for the purpose of calibrating the SGDA :

$$Z_1(\omega) = \frac{P_1(\omega)}{dn / dt(\omega)} : \text{pneumatic impedance of reservoir chamber } Ch_1 \quad (6)$$

$$Z_2(\omega) = \frac{P_2(\omega)}{dn / dt(\omega)} : \text{pneumatic impedance of reaction chamber } Ch_2 \quad (7)$$

$$Z_v(\omega) = \frac{(P_1 - P_2)(\omega)}{dn / dt(\omega)} : \text{pneumatic impedance of needle valve NV} \quad (8)$$

The pneumatic circuit of figure (1) can be modelled using an electrical analogy. When the driving force ΔP^0 used to transfer hydrogen from the reference volume chamber Ch_1 to the reaction chamber Ch_2 is set to a proper value (in practice, < 500 mbar), it can be shown that both reference and reaction chambers behave like electrical capacitances and that the needle valve behaves like an electrical resistance. In that case, equations (6), (7) and (8) take the analytical form [5] :

$$Z_1(\omega) = R_v - j \frac{1}{\omega C} \quad (9)$$

$$Z_2(\omega) = -j \frac{1}{\omega C} \quad (10)$$

$$Z_3(\omega) = R_v \quad (11)$$

$$\text{where : } \begin{cases} R_v = \frac{R T}{K_v P_1^0} \equiv Pa.s.mol^{-1} \\ C = \frac{V}{R T} \equiv mol.Pa^{-1} \end{cases} \quad (12)$$

K_V is a valve constant (from Poiseuille's law [5]), R the gas constant and T the absolute temperature. Eq. (9) is the expression of the impedance for the series connection of a resistor and a capacitor. Because of gas compressibility, the value of R_V in Eq. (12) is a function of the limit pressure value P_1^0 . The higher the pressure of transfer, the higher the gas flow is and thus, the lower the pneumatic resistance. The low frequency behaviour is that of a capacitor, the capacitance C which is related to the volume of the chambers (V) through Eq. (12). Eq. (10) is the impedance of a pure capacitance related to V , the volume of the reaction chamber. And finally, Eq. (11) is the expression of the impedance of a pure resistor, the pneumatic impedance associated with the needle valve. The corresponding graph in Nyquist co-ordinates is a single point located on the real axis, independent of the pulsation ω . The precision obtained on the experimental pneumato-chemical impedances is directly related to the precision of the volumes of the different chambers and the needle valve. Accurate calibration procedures are therefore needed.

2.4. Calibration procedures

During calibration experiments, the reaction chamber is left empty and hydrogen is transferred from Ch_1 to Ch_2 . The driving force for the transfer is the initial pressure difference $\Delta P^0 = P_1^0 - P_2^0$ set between the two chambers. At the opening of MV_2 , hydrogen is transferred from one chamber to the other until the pressure becomes uniform in the two chambers. The volume chambers and the needle valve of the experimental setup are calibrated using the law of perfect gases. The hydrogen mass flow is not directly measured. It can be either deduced from $P_1(t)$:

$$\frac{dn}{dt}(t) = \frac{V_{Ch1}}{RT} \frac{dP_1}{dt}(t) \quad (13)$$

or calculated from $P_1(t)$ and $P_2(t)$ using Poiseuille's law (the needle valve behaves like a tube of uniform section which follows Poiseuille's law) :

$$\frac{dV}{dt}(t) = \frac{([P_1(t)]^2 - [P_2(t)]^2) \pi r^4}{16 \eta P_0 L} \quad (14)$$

where V is the volume of gas of viscosity η transferred at pressure P_0 along a tube of length L and radius r . Assuming that hydrogen behaves ideally (this is justified for systems with plateau pressure values up to a few bars such as those considered here) and that there is no heat effects, the transient hydrogen mass flow $dn/dt(t)$ is then given by :

$$\frac{dn}{dt}(t) = \frac{K_V}{RT} ([P_1(t)]^2 - [P_2(t)]^2) \quad (15)$$

$$\text{where } K_V = \frac{\pi r^4}{16 \eta L} \quad (16)$$

, which is homogeneous to the $m^3 \cdot Pa^{-1} \cdot s^{-1}$ scale, is a constant characterizing the needle valve.

Experimental transient values of $P_1(t)$, $P_2(t)$, $\Delta P(t) = P_1(t) - P_2(t)$ and $dn/dt(t)$ can be fitted using analytical expressions derived elsewhere [5] as a function of the different parameters of the system (K_V , V_1 , V_2 , P_1^0 , P_2^0) :

$$P_1(t) = \frac{(V_1 P_1^0 + V_2 P_2^0)}{(V_1 - V_2)} \left[\frac{1 + \frac{(P_1^0 + P_2^0)}{(P_1^0 - P_2^0)} e^{\alpha t}}{1 + \frac{(V_1 + V_2)(P_1^0 + P_2^0)}{(V_1 - V_2)(P_1^0 - P_2^0)} e^{\alpha t}} \right] \quad (17)$$

$$P_2(t) = \frac{V_1}{V_2} [P_1^0 - P_1(t)] + P_2^0 = \frac{V_1}{V_2} \left[P_1^0 - \frac{(V_1 P_1^0 + V_2 P_2^0)}{(V_1 - V_2)} \left[\frac{1 + \frac{(P_1^0 + P_2^0)}{(P_1^0 - P_2^0)} e^{\alpha t}}{1 + \frac{(V_1 + V_2)(P_1^0 + P_2^0)}{(V_1 - V_2)(P_1^0 - P_2^0)} e^{\alpha t}} \right] \right] + P_2^0 \quad (18)$$

$$\Delta P(t) = P_1(t) - P_2(t) = P_1(t) \left[1 + \frac{V_1}{V_2} \right] - \frac{V_1}{V_2} P_1^0 - P_2^0$$

$$= \frac{(V_1 + V_2)}{V_2} \frac{(V_1 P_1^0 + V_2 P_2^0)}{(V_1 - V_2)} \left[\frac{1 + \frac{(P_1^0 + P_2^0)}{(P_1^0 - P_2^0)} e^{\alpha t}}{1 + \frac{(V_1 + V_2)}{(V_1 - V_2)} \frac{(P_1^0 + P_2^0)}{(P_1^0 - P_2^0)} e^{\alpha t}} \right] - \frac{V_1}{V_2} P_1^0 - P_2^0 \quad (19)$$

$$\frac{dn(t)}{dt} = + \frac{4 K_V}{R T} \frac{(V_1 P_1^0 + V_2 P_2^0)^2}{(V_1 - V_2)^2} \frac{(P_1^0 + P_2^0)}{(P_1^0 - P_2^0)} \left[\frac{e^{\alpha t}}{\left(1 + \frac{(V_1 + V_2)}{(V_1 - V_2)} \frac{(P_1^0 + P_2^0)}{(P_1^0 - P_2^0)} e^{\alpha t} \right)^2} \right] \quad (20)$$

$$\text{where } \alpha = + 2 K_V \left[\frac{P_1^0}{V_2} + \frac{P_2^0}{V_1} \right] \quad (21)$$

As can be seen from Figure 3, the kinetics of gas transfer from Ch_1 to Ch_2 increases with K_V . An optimum value of K_V must be found to perform PIS measurements when a hydrogen absorbing sample is introduced in the reaction chamber. Figure 4 shows that the shape of the pressure response $P_2(t)$ during absorption is a function of K_V . The value of K_V must be adjusted to separate high (HF) and low (LF) frequency contributions, as discussed in [7].

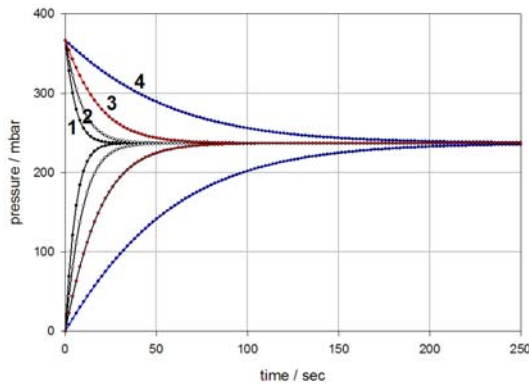


Figure 3 : transient pressures $P_1(t)$ and $P_2(t)$ calculated from Eqs. (17) and (18).

1. $K_V = 1 \times 10^{-10}$; 2. $K_V = 2.6 \times 10^{-11}$;
3. $K_V = 3 \times 10^{-11}$; 4. $K_V = 1 \times 10^{-11} \text{ m}^3 \cdot \text{Pa}^{-1} \cdot \text{s}^{-1}$.

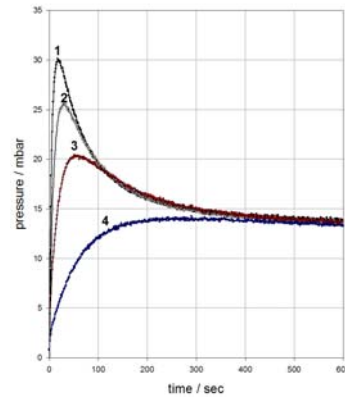


Figure 4 : experimental $P_2(t)$ measured at $H/M = 0.05$ for different position of the needle valve; 1. one; 2. two; 3. three and 4. four graduations.

3. PIS analysis of hydrogen sorption : the $\text{LaNi}_5\text{-H}_2(\text{g})$ system in the low concentration domain during activation

PIS can be used to analyze the dynamics of hydrogen sorption by IMC. This is exemplified in the present communication by considering the activation of the $\text{LaNi}_5\text{-H}_2(\text{g})$ system at 298 K.

3.1. Thermodynamics

Figure 5 shows experimental isotherms measured at 298 K in the low hydrogen concentration domain ($H/M < 1.5$) during the activation procedure. It is known from the literature that during the first hydriding cycles, deprecipitation phenomena occur : precipitation of the hydride phase generates internal defects which in turn induce the pulverisation of the sample into a fine powder. It can be seen from figure 5 that the absorption plateau pressure decreases as the number of hydriding / dehydriding cycles increases (the whole isotherms up to $H/M \approx 6$ are not represented). A question of interest is to determine whether there exist any relationship between thermodynamic states and sorption kinetics or not. If yes, what is the reaction step (surface chemisorption or bulk transport of hydrogen by diffusion) which is mostly affected by this evolution. To answer this question, experimental impedance diagrams must be measured during the activation process.

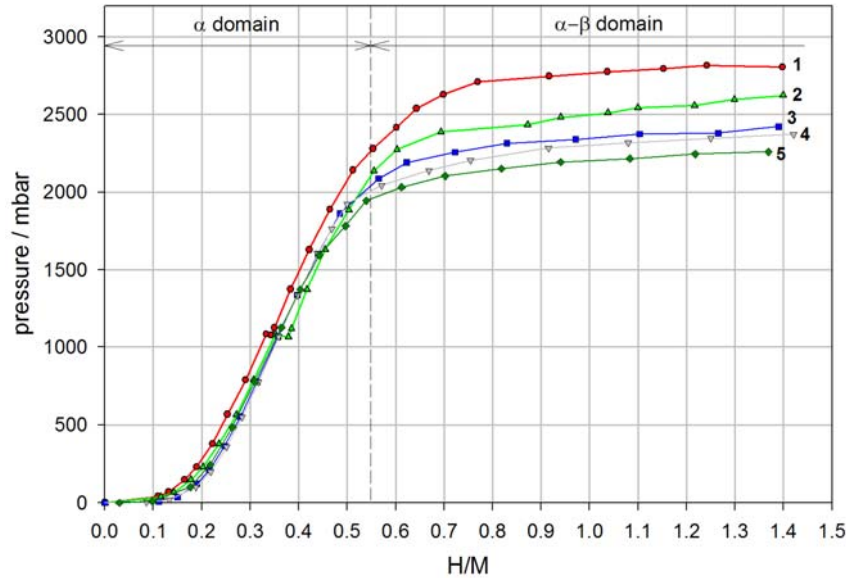


Figure 5 : isotherms of the $\text{LaNi}_5\text{-H}_2(\text{g})$ system measured at 298 K in the low hydrogen concentration domain during 5 successive cycles of absorption.

3.2. Fourier domain analysis of the sorption kinetics

Eq. (7) can be used to obtain experimental pneumato-chemical impedances associated with the reaction chamber, in order to analyze the dynamics of hydrogen absorption in the frequency domain. Such impedance diagrams are obtained as follow. As discussed in the experimental section, kinetic data is collected by sequentially transferring hydrogen amounts from the reference to the reaction chamber. By adjusting the initial pressure P_1^0 , it is possible to obtain the desired composition step $\Delta(H/M)$. Typically, $0.02 < \Delta(H/M) < 0.2$. Thus doing, isothermal and non-convective gas transfer experiments are performed. Figure 6 shows the transient pressure signals sampled during a typical gas transfer experiment. These signals provide the raw data from which experimental transfer functions are obtained using Eq. (7). Assuming that hydrogen behaves like an ideal gas (this is justified here at operating pressures below 3 bars), dn/dt is obtained by derivation of $P_1(t)$. Then $P_2(t)$ and $dn/dt(t)$ are numerically Fourier transformed and the complex ratio is calculated over the corresponding frequency domain. The resulting pneumato-chemical impedance is plotted in Nyquist coordinates (real part vs. imaginary part) in figure 6 where pnohm ($\text{Pa}\cdot\text{mol}^{-1}\cdot\text{s}$) is used for “pneumatocal ohm”, to underline the similarity between electrochemical and gas-phase impedances.

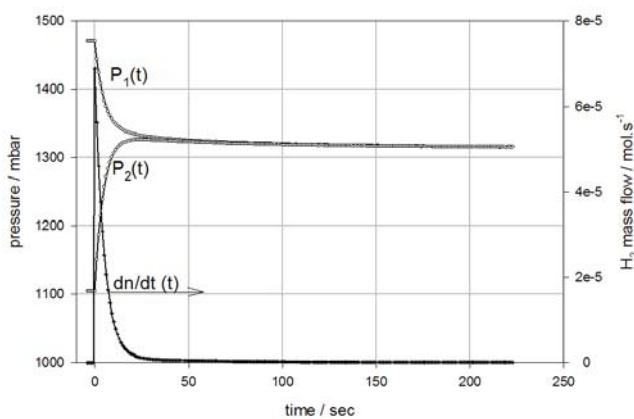


Figure 6 : experimental transient pressure and mass flow signals measured on LaNi_5 at 298 K, in the solid solution domain ($H/M = 0.31 \rightarrow 0.35$).

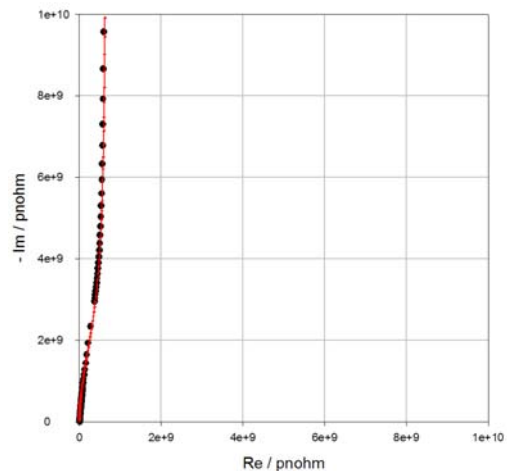
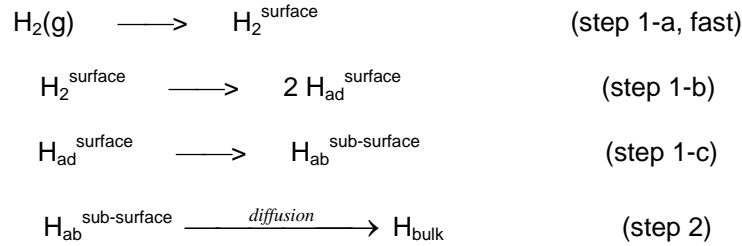


Figure 7 : experimental (●) and model (—) pneumato-chemical impedances obtained from the data of figure 6 and model equations ($1 \text{ Hz} < f < 1 \times 10^{-4} \text{ Hz}$).

3.2. Modelling

When hydrogen absorption occurs from the gas phase and when a solid solution is formed, the following reaction path should be considered [8] :



where H_{ad} denotes a surface ad-atom and H_{ab} denotes a hydrogen atom absorbed in the metal sub-surface. Step 2 corresponds to the diffusion-controlled transport of hydrogen atoms to bulk regions. In two-phase domains, an additional step of hydride precipitation (not considered here), appears. The reader interested in modelling hydriding reactions in two-phase domains may consult Ref. [9].

In a first approximation, a pneumatic resistance R_s can be attributed to steps (1-b) and (1-c) and a diffusion impedance can be attributed to step (2). Therefore, the pneumato-chemical transfer function of the system $Z(\omega)$ is that of the series connection of a surface resistance R_s and a diffusion impedance Z_D in parallel with the capacitance of the reaction chamber :

$$Z(\omega) = R_{NV} + \left[\frac{1}{jC_{Ch_2} \omega + \left(\frac{1}{R_s + Z_D} \right)} \right] \quad (22)$$

where : R_{NV} is the pneumatic resistance of the needle valve ; C_{Ch_2} is the capacitance of the reaction chamber Ch_2 ; R_s is the surface resistance associated with the chemisorption process (steps 1-b, 1-c) and Z_D (step 2) is the classical diffusion impedance [10,11] adapted [12] to solid-gas reactions. Considering the powder morphology of the sorbing IMC, it is logical to choose for Z_D the analytical solution obtained for diffusion in spherical coordinates :

$$Z_D^{C, \text{sphère}}(s) = \frac{r}{D_H} \frac{\partial P_{H_2}}{\partial C_H} \frac{1}{[u \coth(u) - 1]} = R_D^{C, \text{sphère}} \frac{1}{[u \coth(u) - 1]} \quad (23)$$

$$\text{where } R_D^{C, \text{sphère}} = \frac{r}{D_H} \frac{\partial P_{H_2}}{\partial C_H}, \quad u = \sqrt{\frac{s r^2}{D_H}} \quad (24)$$

$\frac{\partial P_{H_2}}{\partial C_H}$ is the slope of the isotherm at the measurement point.

Eqs. (22) and (23) were used in this work to fit the experimental pneumato-chemical impedance of figure 7. Assuming an homogeneous particle radius of ca. 50 μm (estimated from X-ray diffraction measurements), the fit was obtained using $R_s = 6 \times 10^9 \text{ Pa} \cdot \text{mol}^{-1} \cdot \text{s}$ and $D_H = 2 \times 10^{-8} \text{ cm}^2 \cdot \text{s}^{-1}$ at 298 K.

3.3. Frequency domain analysis of the kinetics during the activation procedure

As can be seen from figure 7, the time constant of the two main sorption steps (surface chemisorption and bulk diffusion) are not well separated, yielding additional problems in data fitting. An important criterion which can be used to improve the separation of the high and low frequency contributions is the slope of the isotherm at the measurement point [7,9]. The lower the slope, the better the separation between surface and bulk contribution in Nyquist coordinates. This is why in the present communication, the activation procedure of the sample (figure 5) was followed by measuring the sorption impedance at the foot of the isotherm ($\text{H}/\text{M} \approx 0$), cycle by cycle. This is the point of the isotherms where the slope $dP/d(\text{H}/\text{M})$ is the smallest and where the model (hydrogen diffusion in solid

solutions) applies. Results obtained are plotted in figure 8. A full interpretation of this series of impedance diagrams is beyond the scope of this paper but some comments can be made. Since the capacitance of the reaction chamber expressed by Eq. (12) and the slope of the isotherms at the measurement points are constants for the five impedances of figure 8, the reduction of the real part of the impedance along the number of absorption/desorption process (as shown in figure 8) can be attributed to the reduction of the diffusion impedance. Assuming that the mean hydrogen diffusion coefficient remains constant (same temperature), the reduction of the diffusion impedance must be attributed to the decrease of the diffusion length, *i.e.* to the particle size. Also, the HF semi-circle, although not fully developed, decreases along the activation process. From these observations, it can be concluded that the sorption kinetics increases during the activation procedure. This is because the absorbing sample is pulverized into a fine powder. The total solid-gas interface area increases, the global surface resistance decreases as well as the mean length of the diffusion path. The interest of PIS analysis is that it offers the possibility to separately probe surface and bulk processes and access individual rate parameters for each step of the multi-step hydriding reaction.

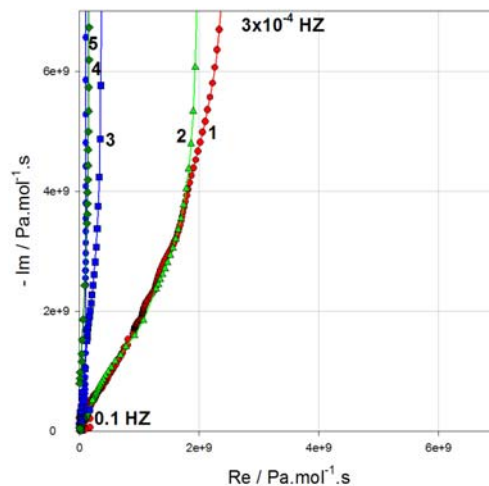


Figure 8 : experimental pneumato-chemical impedances measured at $H/M = 0.0$ during the activation process of figure 5. (1,2,3,4,5) are referring to the experiments of Fig. 5.

The main experimental problem encountered during the analysis of sorption kinetics along the activation process was to obtain homogeneous particle size distributions after each activation cycle, in order to avoid noisy signals and to obtain regularly-shaped impedance diagrams. PIS measurements in non-homogeneous powder beds lead to more or less distorted impedance diagrams and less accurate values of rate parameters compared to bulk materials.

6. Conclusions and perspectives

Derived from electrochemical impedance spectroscopy (EIS), pneumato-chemical impedance spectroscopy (PIS) is a tool which can be used to analyze multi-step reaction mechanisms in solid-gas systems. The practical conditions required to obtain experimental pneumato-chemical impedances from a classical Sievert's-type setup (SGDA) are presented. Experimental PIS diagrams are measured during the activation process of the $\text{LaNi}_5\text{-H}_2(\text{g})$ system. A model based on electrical analogies is used to fit these experimental PIS diagrams. Based on previous analysis, the sorption process is assumed to consist of two successive steps : (i) surface chemisorption of molecular hydrogen and dissociation into hydrogen adatoms and (ii) diffusion-controlled transport of atomic hydrogen to bulk regions. It is found that the impedance related to the hydrogen diffusion process decreases as a function of the number of hydriding cycles, in direct relation with the decrepitation process *i.e.* the reduction of the mean particle diameter. PIS can therefore be used to separately probe surface and bulk modifications during cycling. When a hydride tank based on AB_5 materials is used to store hydrogen from a PEM water electrolyzer, trace amounts of residual oxygen and/or water may contaminate the powder surface and decrease the sorption kinetics [6]. Also, when hydrogen is transferred too rapidly to the reaction chamber, heat effects can irreversibly alter the material and reduce the storage capacity. PIS can be used to quantify these two problems and help to design hydride storage tanks. Detailed results related to these problems cannot be presented within the format of this paper and will be published elsewhere [10].

References

- [1] G.G. Libowitz, H.F. Hayes and T.R.P. Gibb, "The System Zirconium-Nickel and Hydrogen", *J. Phys. Chem.*, 62, 76-79, (1958)
- [2] J.H.N. Van Vucht, F.A. Kuijpers, H.C.A.M. Bruning, *Philips Res. Rep.*, 25, 133, (1970)
- [3] G. Sandrock, G. Thomas, IEA/DOC/SNL on-line hydride database., *Appl. Phys. A*, 72, 153, (2001)
- [4] A. Deschamps, C. Etiévant, P. Millet, C. Puyenchet, « Hydrogen-based electric power unit for domestic applications », *Proceeds. Workshop International sur l'Hydrogène (WIH2)*, Ghardaïa, Algérie, (2007)
- [5] P. Millet, "Pneumatochemical Impedance Spectroscopy. 1. Principles", *J. Phys. Chem. B*, 109, 24016-24024, (2005)
- [6] P. Millet, "Pneumatochemical Impedance Spectroscopy. 2. Dynamics of Hydrogen Sorption by Metals", *J. Phys. Chem. B*, 109, 24025-24030, (2005)
- [7] P. Millet, C. Decaux, R. Ngameni and M. Guymont, "Experimental requirements for measuring pneumato-chemical impedances", *Rev. Sci. Instrum.*, accepted for publication.
- [8] M. Martin, C. Gommel, C. Borkhart, E. Fromm, "Absorption and desorption kinetics of hydrogen storage alloys", *J. Alloys Comp.*, 238, 193-201, (1996)
- [9] P. Millet, C. Decaux, R. Ngameni and M. Guymont, « Fourier-domain analysis of hydriding kinetics using pneumato-chemical impedance spectroscopy », *Res. Letters in Phys. Chem.*, in press
- [10] T. Jacobsen and K. West, "Diffusion impedance in planar, cylindrical and spherical symmetry", *Electrochim. Acta*, 40, 255-262, (1995)
- [11] J.S. Chen, J-P. Diard, R. Durand and C. Montella, "Hydrogen insertion reaction with restricted diffusion. Part 1. Potential step—EIS theory and review for the direct insertion mechanism", *J. Electroanal. Chem.*, 406, 1-13, (1996)
- [12] P. Millet *et al.*, *J. Alloys Comp.*, in preparation